

Article

Effects of Transition Elements on the Structural, Elastic Properties and Relative Phase Stability of L_{12} γ' - Co_3Nb from First-Principles Calculations

Cuiping Wang¹, Chi Zhang¹, Yichun Wang¹, Jiajia Han^{1,*} , Weiwei Xu² and Xingjun Liu^{1,3,4,*}

¹ Fujian Provincial Key Laboratory of Materials Genome, College of Materials, Xiamen University, Xiamen 361005, China; wangcp@xmu.edu.cn (C.W.); xmuzc@stu.xmu.edu.cn (C.Z.); 20720171150094@stu.xmu.edu.cn (Y.W.)

² School of Aerospace Engineering, Xiamen University, Xiamen 361005, China; wwwxu306@xmu.edu.cn

³ State Key Laboratory of Advanced Welding and Joining, Harbin Institute of Technology, Shenzhen 518055, China

⁴ Institute of Materials Genome and Big Data, Harbin Institute of Technology, Shenzhen 518055, China

* Correspondence: jiajiahan@xmu.edu.cn (J.H.); lxj@xmu.edu.cn (X.L.); Tel.: +86-592-218-0606 (J.H. & X.L.)

Abstract: In order to explore novel light-weight Co-Nb-based superalloys with excellent performance, we studied the effects of alloying elements including Sc, Ti, V, Cr, Mn, Fe, Ni, Y, Zr, Mo, Tc, Ru, Rh, Pd, Hf, Ta, W, Re, Os, Ir and Pt on the structural stability, elastic and thermodynamic properties of γ' - Co_3Nb through first-principles calculations. The results of transfer energy indicate that Y, Zr, Hf and Ta have a strong preference for Nb sites, while Ni, Rh, Pd, Ir and Pt have a strong tendency to occupy the Co sites. In the ground state, the addition of alloying elements plays a positive role in improving the stability of γ' - Co_3Nb compound. The order of stabilizing effect is as follows: Ti > Ta > Hf > Pt > Ir > Zr > Rh > V > Ni > W > Sc > Mo > Pd > Re > Ru. Combining the calculation results of elastic properties and electronic structure, we found that the addition of alloying elements can strengthen the mechanical properties of γ' - Co_3Nb , and the higher spatial symmetry of electrons accounts for improving the shear modulus of γ' - Co_3Nb compound. At finite temperatures, Ti, Ta, Hf, Pt, Ir, Zr and V significantly expand the stabilization temperature range of the γ' phase and are potential alloying elements to improve the high-temperature stability of the γ' - Co_3Nb compounds.

Keywords: Co-Nb based superalloys; first-principles calculations; structural stability; mechanical properties



Citation: Wang, C.; Zhang, C.; Wang, Y.; Han, J.; Xu, W.; Liu, X. Effects of Transition Elements on the Structural, Elastic Properties and Relative Phase Stability of L_{12} γ' - Co_3Nb from First-Principles Calculations. *Metals* **2021**, *11*, 933. <https://doi.org/10.3390/met11060933>

Academic Editor: Marcello Cabibbo

Received: 2 April 2021

Accepted: 1 June 2021

Published: 8 June 2021

Publisher's Note: MDPI stays neutral with regard to jurisdictional claims in published maps and institutional affiliations.



Copyright: © 2021 by the authors. Licensee MDPI, Basel, Switzerland. This article is an open access article distributed under the terms and conditions of the Creative Commons Attribution (CC BY) license (<https://creativecommons.org/licenses/by/4.0/>).

1. Introduction

With the continuous development of modern aviation industry, Ni-based superalloys cannot meet the increasing performance needs because their operating temperature is close to the melting point. Therefore, the development of the superalloys that have a higher melting point becomes an urgent task [1,2]. Co-based superalloys are expected to be the next generation of commercial superalloys owing to the higher melting point of Co compared to Ni (1495 °C vs. 1455 °C). In 2006, Sato et al. [3] discovered the Co-Al-W ternary superalloy system, where coherent γ' - $\text{Co}_3(\text{Al}, \text{W})$ precipitates from the γ -Co matrix. The microstructure of γ/γ' two-phase equilibrium, which is extremely similar to that in commonly used Ni-based superalloys, allows Co-Al-W superalloys to exhibit excellent high-temperature mechanical properties while having a high melting point [4–6]. However, due to the high content of heavy element W, the density of Co-Al-W superalloys is much higher (9.5 g/cm³ for Co-9Al-9W) than that of Ni-based superalloys (~8.5 g/cm³), which limits the practical application of Co-Al-W superalloys [7,8]. In order to explore W-free type Co-based superalloys, numerous experiments have been carried out with great progress in recent years, and γ/γ' two-phase microstructure was found in Co-Al-Mo-Nb/Ta [9,10], Co-Ti-Mo [11], Co-Ti-Cr [12], Co-Ti-V [13], Co-V-Ta [14–16], and Co-Al-V [17].

Recently, from more than 200 of 1000 potential compounds, Kirklın et al. [18] predicted that Co_3X ($\text{X} = \text{Ti}, \text{V}, \text{Ta}, \text{W}, \text{Pt}, \text{Ge}, \text{Ga}, \text{Si}, \text{and Nb}$) contains L1_2 precipitates by high-throughput computational methods and conjectured that ternary L1_2 phase could be obtained by combining these alloy elements. After that, Nyshadham et al. [19] predicted the existence of γ/γ' microstructure in Co-Nb-V ternary systems by using a similar theoretical method, which was confirmed by subsequent experimental study [14]. As reported, γ' phase in Co-Nb-V ternary system is metastable, which would decompose to D0_{19} structure after short aging time. The addition of alloying elements can significantly improve the properties of the alloy, which is an effective way to improve the performance defects of the new Co-based superalloy. Moreover, transition metal elements are common alloying elements in the research of new Co based superalloys. For instance, the addition of Ti, V, Ni, Mo, Ru, Ta and Ir can improve the thermal stability and volume fraction of γ' phase [20]; the addition of Zr and Hf can improve the grain boundary bonding strength and enhance the ductility of the alloy [21,22]. Cr plays an important role in improving the oxidation resistance, reducing the alloy density and γ/γ' phase mismatch [23]. As an emerging basic system, the effect of alloying transition elements on the properties of γ' - Co_3Nb phase is fundamentally not clear, and there is little relevant report on this low-density system. Therefore, further research on Co-Nb-based superalloys is of great significance for the development of light-weight superalloys.

In this work, the alloying effect of transition metal elements (X) including Sc, Ti, V, Cr, Mn, Fe, Ni, Y, Zr, Mo, Tc, Ru, Rh, Pd, Hf, Ta, W, Re, Os, Ir and Pt on γ' - Co_3Nb were investigated. Specifically, the atomic configurations of X-substituted γ' - Co_3Nb were determined according to the site preference of transition metal element X in γ' - Co_3Nb , and on this basis, the structural stability and mechanical properties of ternary X-substituted γ' - Co_3Nb were evaluated. By considering the contribution of entropy, the stable temperature range of γ' - Co_3Nb phase against D0_{19} phase is determined, which provides a theoretical basis for the development of the ternary light-weight Co-based superalloy base alloy system.

2. Materials and Methods

2.1. Site Preference Criteria

As showed in Figure 1, we adopted a $2 \times 2 \times 2$ supercell of 32 atoms to represent γ' - Co_3Nb in this work and its chemical formula is $\text{Co}_{24}\text{Nb}_8$. The labeled sphere represents the Co site and Nb site, which can be substituted by one transition metal element X, resulting in compositions of $(\text{Co}_{23}\text{X}_1)\text{Nb}_8$ and $\text{Co}_{24}(\text{Nb}_7\text{X}_1)$, respectively.

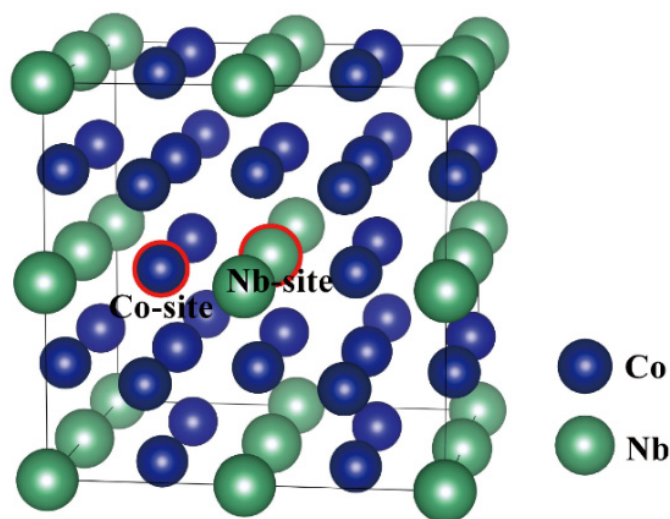


Figure 1. Co_3Nb compound with L1_2 structure. The marked balls represent sites substituted by transition metal X.

We introduce transfer energy $E_X^{\text{Co} \rightarrow \text{Nb}}$ and exchange antisite energy E^{ant} [24,25] to explore the site preference of ternary alloying elements in γ' -Co₃Nb. $E_X^{\text{Co} \rightarrow \text{Nb}}$ characterizes the energy required in moving an X atom from the Co sublattice to the Nb sublattice at 0 K. $E_X^{\text{Co} \rightarrow \text{Nb}}$ and E^{ant} can be calculated as:

$$E_X^{\text{Co} \rightarrow \text{Nb}} = E(\text{Co}_{24}(\text{Nb}_7\text{X}_1)) + E((\text{Co}_{23}\text{Nb}_1)\text{Nb}_8) - E((\text{Co}_{23}\text{X}_1)\text{Nb}_8) - E(\text{Co}_{24}\text{Nb}_8) \quad (1)$$

$$E^{\text{ant}} = E(\text{Co}_{24}(\text{Nb}_7\text{Co}_1)) + E((\text{Co}_{23}\text{Nb}_1)\text{Nb}_8) - 2E(\text{Co}_{24}\text{Nb}_8) \quad (2)$$

where $E(\text{Co}_{24}(\text{Nb}_7\text{X}_1))$, $E((\text{Co}_{23}\text{X}_1)\text{Nb}_8)$ and $E(\text{Co}_{24}\text{Nb}_8)$ are the total energies of compounds $\text{Co}_{24}(\text{Nb}_7\text{X}_1)$, $(\text{Co}_{23}\text{X}_1)\text{Nb}_8$ and $\text{Co}_{24}\text{Nb}_8$, respectively; $E(\text{Co}_{24}(\text{Nb}_7\text{Co}_1))$ and $E((\text{Co}_{23}\text{Nb}_1)\text{Nb}_8)$ are the total energies of Co₃Nb with one Co antisite and one Nb anti-site, respectively. By normalizing the transfer energy, one parameter $\bar{E}_X^{\text{Co} \rightarrow \text{Nb}} = \frac{E_X^{\text{Co} \rightarrow \text{Nb}}}{E^{\text{ant}}}$ is obtained, which can be used to classify the site preference as follows [25]:

- (1) strong Nb site preference ($\bar{E}_X^{\text{Co} \rightarrow \text{Nb}} < 0$);
- (2) weak Nb site preference ($0 < \bar{E}_X^{\text{Co} \rightarrow \text{Nb}} < 0.5$);
- (3) weak Co site preference ($0.5 < \bar{E}_X^{\text{Co} \rightarrow \text{Nb}} < 1$);
- (4) strong Co site preference ($\bar{E}_X^{\text{Co} \rightarrow \text{Nb}} > 1$).

2.2. Stable Formation Energy

With the determination of the site preferences of alloying elements X in γ' -Co₃Nb compounds, the relative phase stability at 0 K could then be evaluated by the stable formation energy (E_{stab}) which is defined as [26]:

$$E_{\text{stab}} = E_{\text{tot}} - \sum_i n_i E_i \quad (3)$$

In particular, when transition elements X occupies Nb site and Co site, the formulas are:

$$E_{\text{stab}}^{\text{XNb}} = E(\text{Co}_{24}(\text{Nb}_7\text{X}_1)) - 7E(\text{Co}_3\text{Nb}) - 3E(\text{Co}) - E(\text{X}) \quad (4)$$

$$E_{\text{stab}}^{\text{XCo}} = E((\text{Co}_{23}\text{X}_1)\text{Nb}_8) - \frac{23}{3}E(\text{Co}_3\text{Nb}) - \frac{1}{3}E(\text{Nb}) - E(\text{X}) \quad (5)$$

respectively, where $E(\text{Co}_3\text{Nb})$ is the total energy of hP24-Co₃Nb, $E(\text{Co})$ is the total energy of hcp-Co and $E(\text{X})$ is the total energy of X in its most stable state. This investigation does not consider whether a solution of X in the Co-matrix may be more stable. Taking Ta occupying Nb site as an example, if the stable formation energy is negative, $E_{\text{stab}}^{\text{TaNb}} < 0$, it indicates that Ta tends to stabilize γ' -Co₃Nb rather than the mixture of three phases (i.e., hP24-Co₃Nb + hcp-Co + bcc-Ta). A larger negative E_{stab} means that the formed phase is more stable; whereas if $E_{\text{stab}}^{\text{TaNb}} > 0$, it indicates that Ta is unfavorable to the stability of γ' -Co₃Nb, and it is difficult to form Ta-substituted Co₃Nb phase compared with the mixture of three phases.

2.3. Elastic Properties

The elastic properties of alloys can be evaluated on the basis of elastic stiffness constants C_{ij} 's. The values of C_{ij} 's at equilibrium were calculated by employing stress-strain method proposed by Shang et al. [27]. A given set of strains $\varepsilon = (\varepsilon_1, \varepsilon_2, \varepsilon_3, \varepsilon_4, \varepsilon_5, \varepsilon_6)$ (where ε_1 - ε_3 refer to normal strains and ε_4 - ε_6 refer to shear strains) was imposed on the crystal to generate the slight deformations. Then, one corresponding set of stress $\sigma = (\sigma_1, \sigma_2, \sigma_3, \sigma_4, \sigma_5, \sigma_6)$ of the

deformed crystal can be obtained by first-principles calculations. In the present work, the linearly independent sets of strain were used as:

$$\begin{pmatrix} x & 0 & 0 & 0 & 0 & 0 \\ 0 & x & 0 & 0 & 0 & 0 \\ 0 & 0 & x & 0 & 0 & 0 \\ 0 & 0 & 0 & x & 0 & 0 \\ 0 & 0 & 0 & 0 & x & 0 \\ 0 & 0 & 0 & 0 & 0 & x \end{pmatrix} \quad (6)$$

with $x = \pm 0.01$. Through the n sets of strain and their corresponding stresses, the elastic stiffness can be calculated based on Hooke's law. According to the symmetry of $L1_2$ -type crystal structure, the number of independent components of elastic stiffness tensor decreases to three (C_{11} , C_{12} , C_{44}). However, it is worth noting that the crystal structure of γ' -Co₃Nb with transition element X occupying Nb site still maintains the original cubic symmetry. When Co is substituted by transition elements X, the cubic supercell of γ' -Co₃Nb will be slightly distorted, which changes from cubic symmetry to tetragonal symmetry, resulting in the increase of the number of independent C_{ij} 's. Therefore, Hooke's law can be simplified to the following formula by:

$$\begin{pmatrix} C_{11} & C_{12} & C_{13} & 0 & 0 & 0 \\ C_{21} & C_{22} & C_{23} & 0 & 0 & 0 \\ C_{31} & C_{32} & C_{33} & 0 & 0 & 0 \\ 0 & 0 & 0 & C_{44} & 0 & 0 \\ 0 & 0 & 0 & 0 & C_{55} & 0 \\ 0 & 0 & 0 & 0 & 0 & C_{66} \end{pmatrix} = \begin{pmatrix} \varepsilon_{1,1} & & \varepsilon_{1,n} \\ \varepsilon_{2,1} & & \varepsilon_{2,n} \\ \varepsilon_{3,1} & \dots & \varepsilon_{3,n} \\ \varepsilon_{4,1} & & \varepsilon_{4,n} \\ \varepsilon_{5,1} & & \varepsilon_{5,n} \\ \varepsilon_{6,1} & & \varepsilon_{6,n} \end{pmatrix}^{-1} \begin{pmatrix} \sigma_{1,1} & & \sigma_{1,n} \\ \sigma_{2,1} & & \sigma_{2,n} \\ \sigma_{3,1} & \dots & \sigma_{3,n} \\ \sigma_{4,1} & & \sigma_{4,n} \\ \sigma_{5,1} & & \sigma_{5,n} \\ \sigma_{6,1} & & \sigma_{6,n} \end{pmatrix} \quad (7)$$

The average C_{ij} were used, which ensures the comparability of our calculated results:

$$\bar{C}_{11} = \frac{C_{11} + C_{22} + C_{33}}{3}, \quad \bar{S}_{11} = \frac{S_{11} + S_{22} + S_{33}}{3} \quad (8)$$

$$\bar{C}_{12} = \frac{C_{12} + C_{13} + C_{23}}{3}, \quad \bar{S}_{12} = \frac{S_{12} + S_{13} + S_{23}}{3} \quad (9)$$

$$\bar{C}_{44} = \frac{C_{44} + C_{55} + C_{66}}{3}, \quad \bar{S}_{44} = \frac{S_{44} + S_{55} + S_{66}}{3} \quad (10)$$

where S_{ij} 's represents elastic compliance constants, which can be obtained from the inverse matrix of C_{ij} 's. Furthermore, the polycrystalline properties, including the bulk modulus (B), shear modulus (G), Young's moduli (E) and Poisson's ratio (ν), can be calculated by Voigt–Reuss–Hill (VRH) method [28]:

$$B_V = \frac{\bar{C}_{11} + 2\bar{C}_{12}}{3}, \quad B_R = \frac{1}{3\bar{S}_{11} + 6\bar{S}_{12}} \quad (11)$$

$$G_V = \frac{\bar{C}_{11} - \bar{C}_{12} + 3\bar{C}_{44}}{5}, \quad G_R = \frac{5}{4\bar{S}_{11} - 4\bar{S}_{12} + 3} \quad (12)$$

$$B_H = \frac{B_V + B_R}{2}, \quad (13)$$

$$G_H = \frac{G_V + G_R}{2} \quad (14)$$

$$E_H = \frac{9B_H G_H}{3B_H + G_H} \quad (15)$$

$$\nu = \frac{3B_H - 2G_H}{2(3B_H + G_H)} \quad (16)$$

2.4. Details of First-Principles Calculations

Herein, first-principles calculations were performed by Vienna Ab initial Simulation Package (VASP) [29,30] based on the projector augmented wave (PAW) method [31] and density functional theory (DFT) [32]. The exchange and correlation function were described by using the Perdew–Burke–Ernzerhof (PBE) generalized gradient approximation (GGA) [33]. The plane wave basis was truncated at a kinetic energy cutoff of 450 eV to ensure that the total energy of all structures converges within 1 meV/atom. For the k-point sampling, Gamma centered grid of $7 \times 7 \times 7$ for $L1_2$ and $3 \times 3 \times 7$ for $D0_{19}$ was used. The reciprocal space integration was executed with the Methfessel–Paxton technique [33] with a smearing width of 0.20 eV. Throughout the calculations, the convergence thresholds of total energy and the maximum force acting on ions was set to less than 10^{-5} eV/atom and 10^{-2} eV/Å, respectively. The spin polarized calculations were performed due to the ferromagnetic nature of Co.

The conjugate gradient algorithm (IBRION = 2) was employed to optimize the structures, allowing the change of ionic positions, cell shape and cell volume (ISIF = 3). In order to obtain an accurate and stable atomic structure, ISIF = 3/IBRION = 2 was repeatedly used for ion relaxation until the structural optimization converged in only one loop. For evaluating the accuracy of this method, fitting a state equation were performed. By changing the scale factors, 10 structures were selected near the structure optimized with ISIF = 3. Then, the optimization (ISIF = 4) and static calculation were carried out. The P-V data of these structures were fitted with the third-order Birch–Murnaghan equation of state to find total energy at the lowest point. The difference in total energy calculated by two methods is about 0.2 meV/atom, which ensures the accuracy of the structure.

When calculating the energy of pure elements, the most stable structures at 293 K and 1 atm were employed as the initial structure. For Ni, Rh, Pd, Ir and Pt with fcc structure containing 4 atoms, a gamma centered $14 \times 14 \times 14$ k-point mesh was adopted; for V, Cr, Fe, Nb, Mo, Ta and W with bcc structure containing 2 atoms, a gamma centered $18 \times 18 \times 18$ k-point mesh was adopted; for Sc, Ti, Co, Y, Zr, Tc, Ru, Hf, Re and Os with hcp structure containing 2 atoms, a gamma centered $23 \times 23 \times 12$ k-point mesh was adopted. Mn has a complicated structure of 58 atoms, and a gamma centered $6 \times 6 \times 6$ k-point mesh was used due to its large unit cell. In particular, Cr was initialized with an anti-ferromagnetic state.

3. Results and Discussion

3.1. Site Preference and Structural Stability

Figure 2 plots the normalized transfer energy of X-substituted γ' -Co₃Nb compounds, which reveals the site preference of transition metal X in γ' -Co₃Nb compounds, and their corresponding values of $E_X^{\text{Co} \rightarrow \text{Nb}}$ are listed in Table 1. It can be seen from Figure 2 that Y, Zr, Hf and Ta have a strong Nb-site preference, while Sc, Ti, V, Cr, Mo, W and Re have a weak Nb-site preference; Mn, Fe, Tc, Ru and Os have a weak Co-site preference, while Ni, Rh, Pd, Ir and Pt have a strong Co-site preference. It is apparent that the site preference shows regular variation according to the periodic table of the elements, i.e., the tendency of elements to occupy Co site becomes progressively stronger with increasing atomic number in each period, which is similar to the findings in the Ni₃Al phase [24].

The lattice parameter is an important physical quantity for the γ' -strengthened super-alloys, which determines the degree of lattice mismatch between the γ' -Co₃Nb precipitate and the γ -Co matrix, and thus controls the morphology and strength of the γ' -Co₃Nb precipitate. The addition of transition element X will cause different degrees of changes in the lattice parameters of γ' -Co₃Nb. Figure 3 illustrates the relationship between the lattice parameters of X-substituted γ' -Co₃Nb and the atomic radius of X. The atomic radius of X is metallic radius, taking from Reference [34]. It can be seen that the lattice parameter of γ' -Co₃Nb is roughly proportional to the atomic radius of element X, which leads to a lattice mismatch of 2.60% ~ 3.72% between the X-substituted γ' -Co₃Nb and the γ -matrix (lattice parameter is 3.52Å). Although the degree of mismatch in the present Co-Nb-X

system is much larger than that of a typical Ni-based superalloy (about 0.5%) [35], the γ'/γ two-phase microstructure can still be formed in the Co-Nb-based system [14].

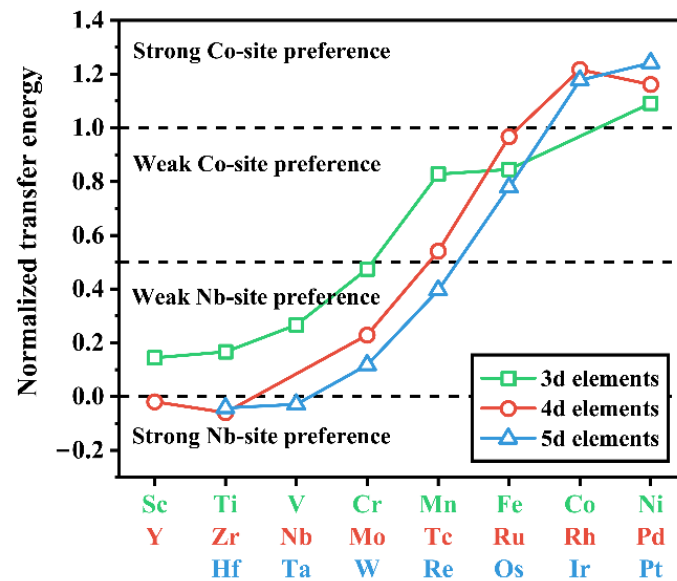


Figure 2. Normalized transfer energy of X-substituted $L1_2$ Co_3Nb compounds.

Table 1. Calculated formation enthalpies (ΔH), lattice constants (a), transfer energy ($E_X^{Co \rightarrow Nb}$) and stable formation energy (E_{stab}) of X-substituted γ' - Co_3Nb compounds. The formation enthalpies (ΔH) is given by the difference in total energy of the compound and that of the corresponding component in their stable solid state. Transfer energy ($E_X^{Co \rightarrow Nb}$) is given by Equation (1). Stable formation energy (E_{stab}) is calculated by Equations (4) and (5), depending on X substituting Co or Nb, respectively.

Compounds	Designation	ΔH (eV/atom)	a (Å)	$E_X^{Co \rightarrow Nb}$ (meV/atom)	E_{stab} (meV/atom)
$Co_{24}Nb_8$	Pure	-0.166	3.631		-0.166
$Co_{24}Nb_7Sc$	Sc_{Nb}	-0.153	3.633	11.739	-7.963
$Co_{24}Nb_7Ti$	Ti_{Nb}	-0.176	3.626	13.505	-31.313
$Co_{24}Nb_7V$	V_{Nb}	-0.162	3.612	21.646	-16.941
$Co_{24}Nb_7Cr$	Cr_{Nb}	-0.135	3.613	38.490	9.675
$Co_{23}Nb_8Mn$	Mn_{Co}	-0.155	3.633	67.212	3.931
$Co_{23}Nb_8Fe$	Fe_{Co}	-0.158	3.635	68.573	0.763
$Co_{23}Nb_8Ni$	Ni_{Co}	-0.171	3.631	88.612	-11.596
$Co_{24}Nb_7Y$	Y_{Nb}	-0.118	3.651	-1.538	27.087
$Co_{24}Nb_7Zr$	Zr_{Nb}	-0.164	3.639	-4.861	-19.319
$Co_{24}Nb_7Mo$	Mo_{Nb}	-0.150	3.626	18.619	-5.193
$Co_{23}Nb_8Tc$	Tc_{Co}	-0.149	3.645	43.889	10.176
$Co_{23}Nb_8Ru$	Ru_{Co}	-0.161	3.642	78.416	-1.708
$Co_{23}Nb_8Rh$	Rh_{Co}	-0.177	3.642	98.767	-17.892
$Co_{23}Nb_8Pd$	Pd_{Co}	-0.163	3.643	94.219	-4.539
$Co_{24}Nb_7Hf$	Hf_{Nb}	-0.173	3.642	-3.422	-27.839
$Co_{24}Nb_7Ta$	Ta_{Nb}	-0.174	3.633	-2.338	-28.483
$Co_{24}Nb_7W$	W_{Nb}	-0.156	3.624	9.554	-10.630
$Co_{24}Nb_7Re$	Re_{Nb}	-0.147	3.622	32.119	-2.009
$Co_{23}Nb_8Os$	Os_{Co}	-0.157	3.647	63.187	1.863
$Co_{23}Nb_8Ir$	Ir_{Co}	-0.183	3.648	95.558	-23.765
$Co_{23}Nb_8Pt$	Pt_{Co}	-0.186	3.648	100.799	-26.923

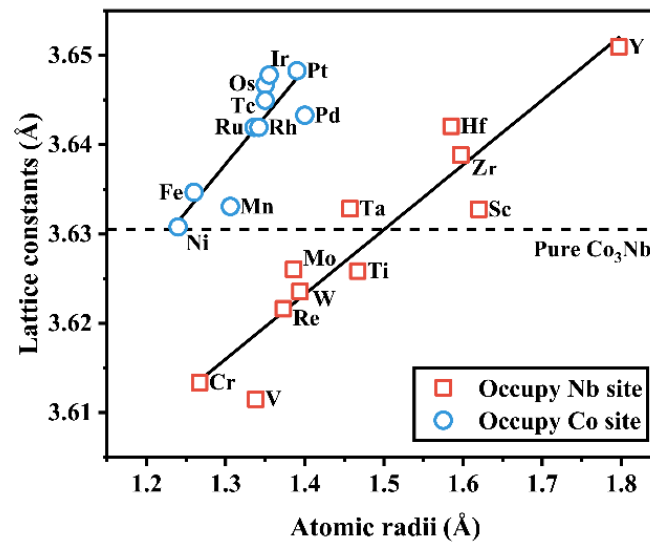


Figure 3. Relationship between the lattice parameters of X-substituted γ' -Co₃Nb and the atomic radius of X.

Based on the site preference of the alloying elements, the stable formation energy E_{stab} was further calculated in order to understand the relative structural stability of X-substituted γ' -Co₃Nb. Figure 4 illustrates the calculated E_{stab} for X-substituted Co₃Nb. It can be seen that the elements of Sc, Ti, V, Ni, Zr, Mo, Ru, Rh, Pd, Hf, Ta, W, Re, Ir and Pt play a positive role in enhancing the structural stability of γ' -Co₃Nb, in the order of Ti > Ta > Hf > Pt > Ir > Zr > Rh > V > Ni > W > Sc > Mo > Pd > Re > Ru. In agreement with the reported experimental and theoretical studies of Co-based superalloys [6,36–38], the addition of Ta and Ti can also greatly improve the structural stability of γ' -Co₃Nb precipitates in the matrix. The results suggest several potential novel γ/γ' Co-Nb-based superalloys, such as Co-Nb-Ti, Co-Nb-Ta and Co-Nb-Hf.

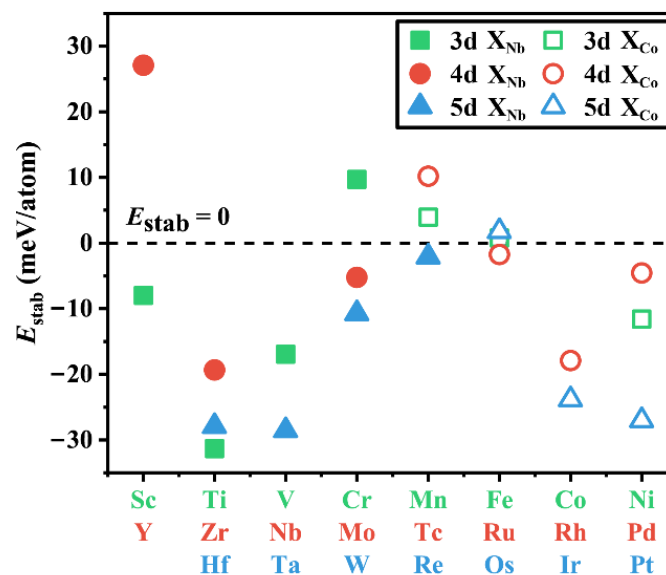


Figure 4. Calculated stable formation energy for γ' -Co₃Nb doped with 3d, 4d and 5d transition metal elements X.

3.2. Alloying Effects on Mechanical Properties

The C_{ij}' s of the X-substituted γ' -Co₃Nb compounds were calculated according to the effective stress–strain method to investigate the effect of alloying element on the elastic

mechanical properties of γ' -Co₃Nb (see Table 2). According to Born's theory [39], the mechanical stability of cubic crystal systems can be determined by the following formula:

$$C_{11} > 0, C_{44} > 0, C_{11} > |C_{12}|, (C_{11} + 2C_{12}) > 0 \quad (17)$$

Table 2. Calculated equilibrium supercell volume (\AA^3) and polycrystalline elastic properties (GPa) of X-substituted γ' -Co₃Nb compounds, including elastic constants (C_{ij}), bulk modulus (B), shear modulus (G), Young's modulus (E), Poisson's ratio (ν), B/G ratio, $C_{12} - C_{44}$, $G_{\{110\}}$ and $G_{\{111\}}$.

X	Volume	C_{11}	C_{12}	C_{44}	B	G	E	ν	B/G	$C_{12} - C_{44}$	$G_{\{110\}}$	$G_{\{111\}}$
Pure	382.81	353	166	159	228	129	325	0.262	1.77	6.19	94	109
Sc	383.53	344	161	161	222	128	323	0.258	1.73	0.28	92	107
Ti	381.35	349	171	158	230	125	318	0.270	1.84	13.18	89	104
V	376.84	368	176	167	240	134	339	0.265	1.79	8.42	96	112
Cr	377.43	365	173	167	237	134	338	0.262	1.77	6.18	96	112
Mn	383.63	349	171	156	230	125	317	0.270	1.85	14.74	89	104
Fe	384.13	347	171	153	230	122	312	0.275	1.88	18.10	88	102
Ni	382.90	357	173	158	234	127	322	0.270	1.85	15.57	92	107
Y	389.32	340	160	152	220	123	311	0.264	1.79	8.19	90	104
Zr	385.46	350	170	158	230	126	320	0.268	1.82	11.54	90	105
Mo	381.40	366	173	166	237	134	338	0.262	1.78	6.82	97	112
Tc	387.40	347	180	157	236	122	311	0.280	1.94	23.31	83	99
Ru	386.44	355	177	161	236	127	323	0.272	1.86	15.63	89	105
Rh	386.44	360	175	160	237	129	326	0.270	1.84	15.04	93	108
Pd	386.86	359	175	158	236	127	323	0.272	1.86	17.12	92	107
Hf	386.48	353	175	156	234	125	318	0.273	1.88	18.33	89	104
Ta	383.56	365	177	162	240	130	331	0.271	1.84	15.49	94	109
W	380.64	371	177	169	241	135	342	0.264	1.78	7.58	97	113
Re	380.02	373	174	168	240	136	344	0.262	1.76	5.27	100	115
Os	387.96	358	184	159	242	124	319	0.281	1.94	25.43	87	102
Ir	388.34	354	170	161	231	129	325	0.265	1.80	8.94	92	107
Pt	388.45	359	171	163	234	131	330	0.264	1.79	8.78	94	109

From Table 2, it can be seen that all X-substituted γ' -Co₃Nb satisfies the above mechanical stability criterion, indicating that they are mechanically stable in the ground state. The polycrystalline elastic mechanical parameters such as bulk modulus B , shear modulus G , Young's modulus E and Poisson's ratio ν calculated for each compound using Voigt–Reuss–Hill scheme [28] are also given in Table 2. In order to investigate the change pattern of elastic properties after the transition metal atom X occupies different sites in γ' -Co₃Nb, the volume change of X-substituted Co₃Nb compounds was plotted in relation to the change of bulk modulus and shear modulus (Figure 5a,b, respectively). As can be seen, the addition of transition elements that preferentially occupy the Co site increases the supercell volume of γ' -Co₃Nb while the opposite is true for elements that tend to occupy the Nb site. This phenomenon can be explained by the atomic radius of transition elements X with respect to the atomic radius of the Co/Nb atom [34]: in general, the radii of alloying atoms (Rh, Ir, Ni, Pd, Pt, etc.) are larger than that of Co atom, but smaller than that of Nb atom. Therefore, the volume of the compound expands when the alloying atoms occupies the Co site and shrinks when the alloying element occupies Nb site. As can be seen from Figure 5, the B and G decrease linearly with the increasing volume when occupying Nb site or Co site, in agreement with previous studies [40]. The addition of transition element V results in the largest volume deformation of the Co₃Nb compound, which led to a large increase in both the elastic modulus and bulk modulus of the Co₃Nb compound. The addition of Ni is effective in increasing the bulk modulus of the Co₃Nb compound even though it hardly changes the volume of the Co₃Nb compound.

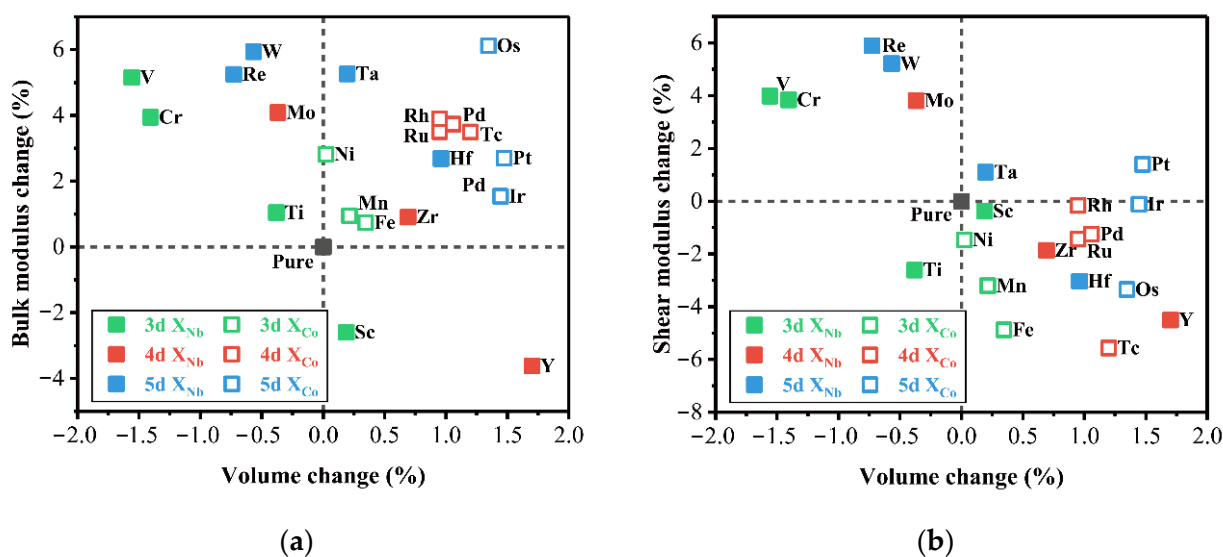


Figure 5. Calculated elastic parameters change as a function of volume change for Co_3Nb compounds with the transition elements X substituted Co and Nb site: (a) bulk modulus B ; (b) shear modulus G . Solid and open symbol represent X prefer to occupy Nb and Co site, respectively.

Then, we predicted the ductile/brittle nature of X-substituted γ' - Co_3Nb by both Pugh's classical criterion (B/G) [41] and Cauchy pressure ($C_{12} - C_{44}$) [42]. The solid materials with B/G greater than 1.75 indicate ductility otherwise brittleness. According to Table 2, the B/G ratio of all X-substituted γ' - Co_3Nb compounds except the element Sc is higher than the critical value of 1.75, indicating that most of the X-substituted γ' - Co_3Nb compounds have good ductility, among which the alloying element such as Tc, Os and Hf significantly improve the ductility of the γ' - Co_3Nb compounds. On the other hand, the Cauchy pressure ($C_{12} - C_{44}$) can be used as an indicator of bonding properties, which can be associated with the Cauchy pressure. A positive value of Cauchy pressure indicates that the system is dominated by metallic bonds, otherwise it is dominated by covalent bonds. For metallic systems, a higher Cauchy pressure represents a more ductile feature. To elucidate the intrinsic relationship between the bonding nature and the ductility/brittleness of materials, the B/G ratio is plotted versus Cauchy pressure ($C_{12} - C_{44}$) in Figure 6. It is clear that there is a linear relationship between the B/G ratio and $C_{12} - C_{44}$. The Cauchy pressure is positive for $B/G > 1.75$, indicating that the ductile characteristics of X-substituted γ' - Co_3Nb are essentially contributed from the metallic bonding nature.

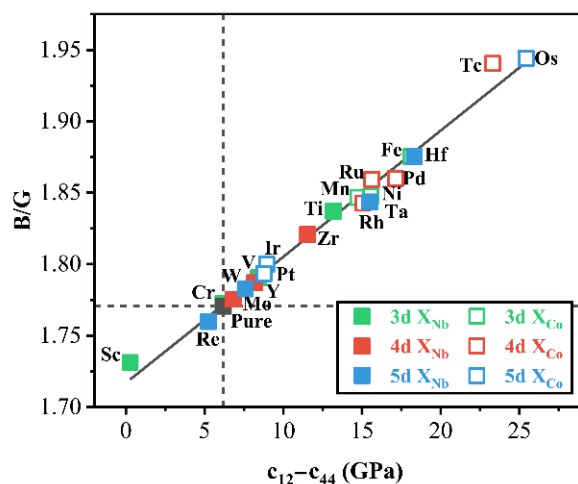


Figure 6. Linear relationship between B/G ratio and $C_{12} - C_{44}$ for the X-substituted γ' - Co_3Nb .

Particularly, three typical mechanical shear moduli, namely $G_{\{100\}}$, $G_{\{110\}}$ and $G_{\{111\}}$ were considered, which represent the shear modulus in the {100} plane along [010] direction, the {110} plane along $[1\bar{1}0]$ direction and the {111} plane along $[11\bar{1}]$ direction, respectively. These shear moduli can be calculated by the following formula [43]:

$$G_{\{100\}} = C_{44} \quad (18)$$

$$G_{\{110\}} = \frac{C_{11} - C_{12}}{2} \quad (19)$$

$$G_{\{111\}} = \frac{3C_{44}(C_{11} - C_{12})}{C_{11} - C_{12} + 4C_{44}} \quad (20)$$

According to the results listed in Table 2, for all X-substituted γ' -Co₃Nb compounds, the shear modulus on each crystal plane satisfies the following relationship: $G_{\{110\}} < G_{\{111\}} < G_{\{100\}}$, which demonstrates that, the X-substituted γ' -Co₃Nb compounds are less resistant to shear sliding in the {110} and {111} planes than that in the {100} plane. By comparing with the shear modulus of the pure γ' -Co₃Nb, we classified these alloying elements into three categories (see Figure 7): (1) Elements that increase the value of $G_{\{110\}}$ and $G_{\{111\}}$, namely V, Cr, Mo, Ta, W, Re and Pt; (2) Elements that substantially decrease the value of $G_{\{110\}}$ and $G_{\{111\}}$, namely Fe, Tc and Os; and (3) Elements that moderately decrease the value of $G_{\{110\}}$ and $G_{\{111\}}$, i.e., Sc, Ti, Mn, Ni, Y, Zr, Ru, Rh, Pd, Hf and Ir.

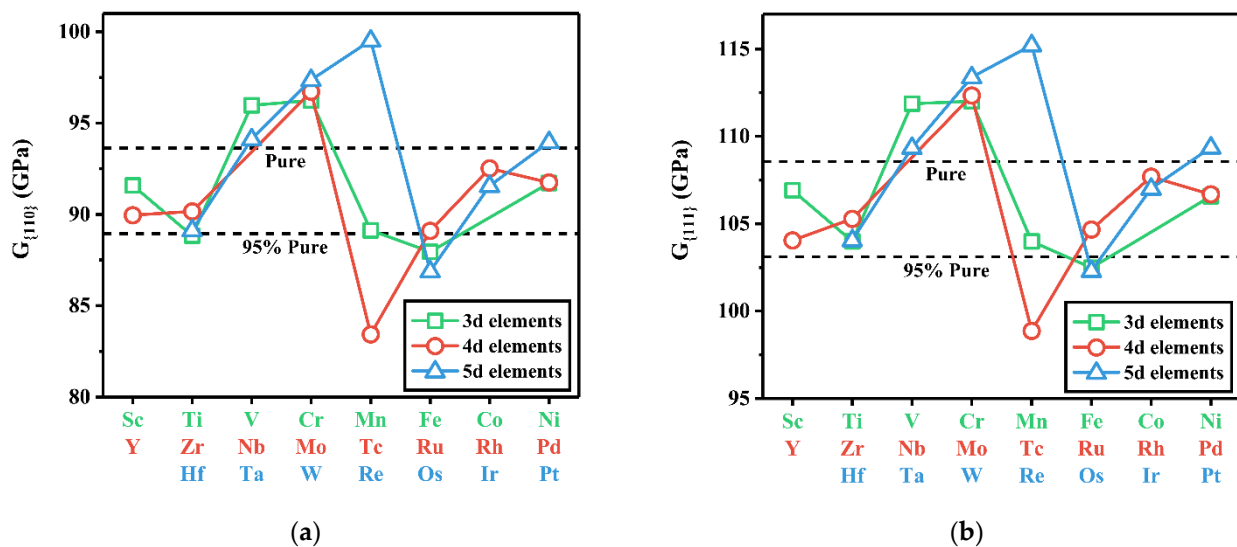


Figure 7. Shear modulus in (a) {110} plane and (b) {111} plane of the X-substituted γ' -Co₃Nb.

3.3. Electronic Structure

According to previous studies [44,45], the valence electrons of compound play a significant role in the shear modulus. Here, we use the charge density difference (CDD) to reveal the relationship between the electronic structure and mechanical properties of the X-substituted γ' -Co₃Nb compounds. The CDD in the (110) plane is intercepted for analysis because of its lowest shear modulus (see Table 2). Figure 8 plots the CDD contours in the (110) plane for Re, Ti, Pt and Tc substitutions, by considering the relatively large and low $G_{\{110\}}$ when Re and Ti occupying the Co site or Pt and Tc occupying the Nb site, respectively.

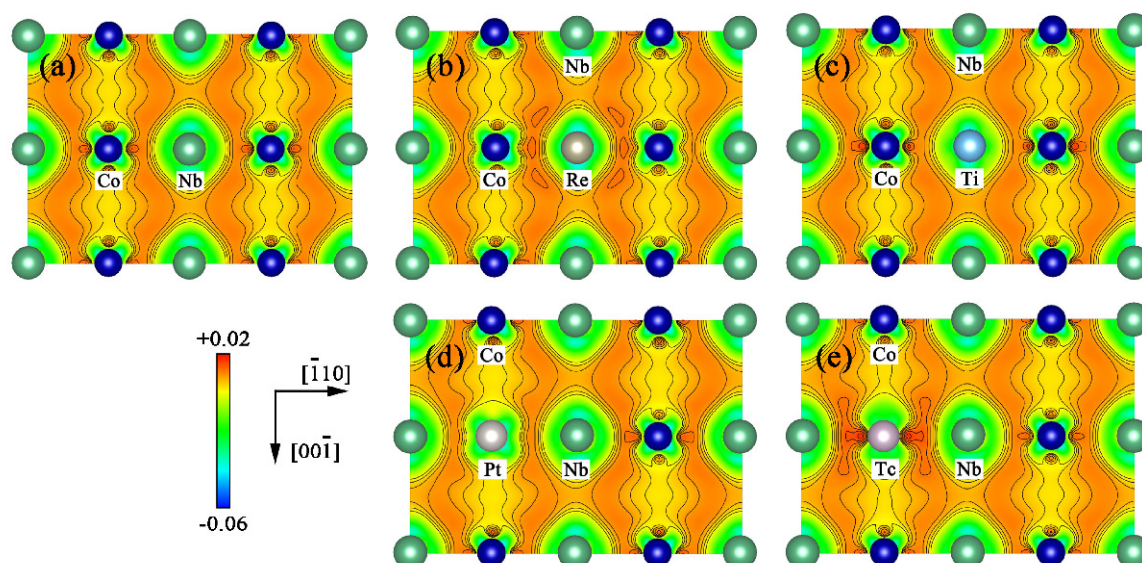


Figure 8. Calculated CDD in the (110) plane for (a) pure, (b) Re-substituted, (c) Ti-substituted, (d) Pt-substituted and (e) Tc-substituted $L1_2$ Co_3Nb , respectively.

From Figure 8a, it can be seen that the transferred electrons of pure γ' - Co_3Nb are mainly distributed between the Co atom and Nb atoms in the (110) plane, which indicates that they form a covalent-like bond. In the case of Re substitution (Figure 8b), transferred electrons homogeneously assemble around the Re atoms, forming a ring-shaped valence bond. This weakens the anisotropy of the (110) plane, and results in an increase in shear modulus on this plane compared with that of pure γ' - Co_3Nb . In Figure 8c, the transferred electrons increase along $[\bar{1}10]$ direction by the substitution of Ti, which leads to a weakened symmetry and thus makes $G_{\{110\}}$ lower. When the Pt atom occupies the Co site as seen in Figure 8d, it has no obvious d-orbital interaction with the surrounding Nb atoms, and the spatial distribution of the transferred electrons is close to γ' - Co_3Nb , so they have comparable values of $G_{\{110\}}$. Furthermore, H-shaped distributed charge can be observed between Tc atoms and two nearest-neighbor Nb atoms as shown in Figure 8e, while the CDD along $[\bar{1}10]$ direction is much more intensive than that along $[00\bar{1}]$ direction. This H-shaped charge distribution increases the anisotropy of bonding, resulting in a significant decrease in $G_{\{110\}}$. It turns out from the above analysis that the ring-shaped electron distribution has a positive effect on the increase of shear modulus.

3.4. Thermodynamic Properties

To consider the influence of temperature on the phase stability and thermodynamic properties of X-substituted γ' - Co_3Nb , the quasi-harmonic Debye model [46] was adopted to evaluate the contribution of entropy to free energy, which can be well implemented by Gibbs2 code [47]. According to Debye model and neglecting the contribution of hot electrons to free energy, the non-equilibrium Gibbs free energy can be expressed as:

$$G^*(V; P, T) = E(V) + F_{vib}(\Theta; T) + PV \quad (21)$$

where $E(V)$ is the static energy and $F_{vib}(\Theta; T)$ is vibrational Helmholtz free energy. At a given temperature T and pressure P , the Gibbs free energy of the equilibrium state can be obtained from the derivative of the Gibbs free energy of the non-equilibrium state to the volume. See [46,47] for more details.

According to a recent experimental study, the γ' - Co_3Nb phase in Co-Nb-V based superalloy will decomposed into $D0_{19}$ phase with increasing annealing time [14]. Therefore, in order to evaluate the phase stability of X-substituted γ' - Co_3Nb at finite temperature, the difference in Gibbs free energy between the $D0_{19}$ phase (Figure S1 provides the supercell of

X-substituted $D0_{19}$ - Co_3Nb and Table S1 provides relevant data of equilibrium state in the Supplementary) and $L1_2$ phase should be considered by the following equation:

$$\Delta G = G_{D0_{19}} - G_{L1_2} \quad (22)$$

where $G_{D0_{19}}$ and G_{L1_2} are the Gibbs free energy of $D0_{19}$ and $L1_2$ structures, respectively. If $\Delta G < 0$, it means that $D0_{19}$ structure is more stable than $L1_2$ structure, and vice versa. Based on the results in Section 3.1, the γ' - Co_3Nb substituted by Ti, Ta, Hf, Pt, Ir, Zr and V elements were, respectively, selected in the calculations, since these compounds have lower stable formation energy E_{stab} than other compounds. Figure 9 depicts the calculated ΔG as a function of temperature for these X-substituted Co_3Nb compounds. It can be seen that Co_3Nb has a negative ΔG over the entire temperature range, which means that γ' - Co_3Nb is a metastable phase relative to the $D0_{19}$ structure. It is noted that the ΔG of X-substituted Co_3Nb is significantly higher than that of Co_3Nb , suggesting that these alloying elements can improve the phase stability of γ' - Co_3Nb at high temperature to a certain extent. Recent experimental studies have verified that the $Co_3(Nb, V)$ is a metastable phase [14], which is consistent with our prediction. According to the results, the addition of Pt, Hf, Ir, Ta and Ti should be more effective than V for improving the stability of γ' - Co_3Nb and can be considered as the potential basic ternary system of X-substituted γ' - Co_3Nb .

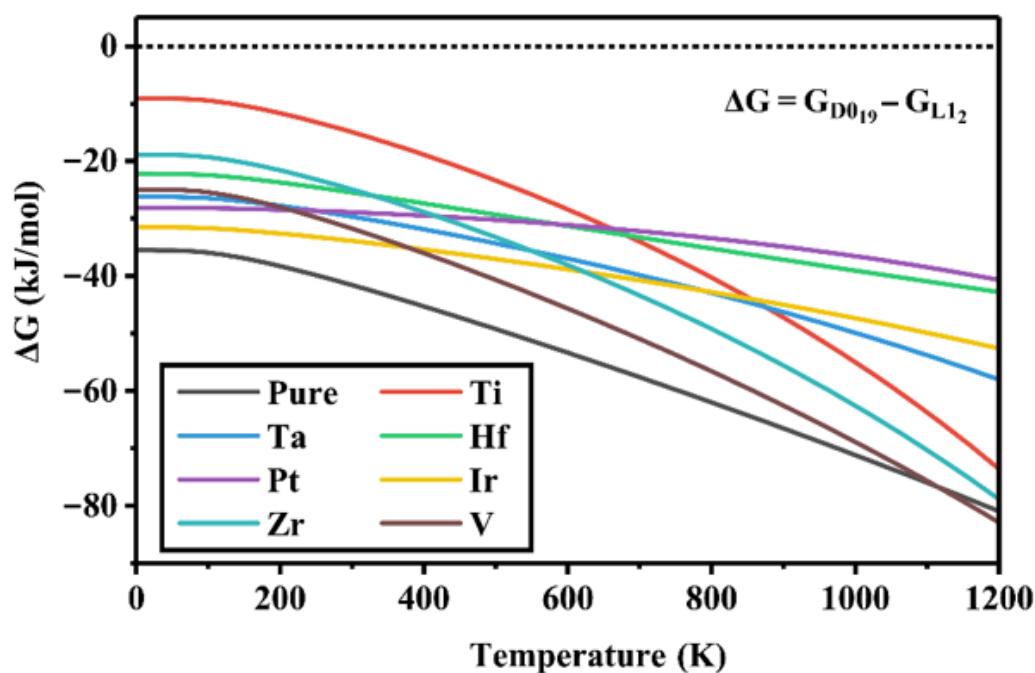


Figure 9. Calculated ΔG of X-substituted Co_3Nb compounds (X = Ti, Ta, Hf, Pt, Ir, Zr, V).

Figure 10a,b illustrates the calculated specific heats of these X-substituted γ' - Co_3Nb compounds at constant pressure (C_p) and constant volume (C_v), respectively. In Figure 10a, the curves show typical feature of specific heat, that is, C_v of these compounds is proportional to T^3 ($C_v \propto T^3$) at low temperatures (<300 K), and tends to Dulong–Petit limit of $C_v = 3nR = 800 \text{ J/K} \cdot \text{mol}$ at high temperatures. C_p depicted in Figure 10b, is larger than C_v over the entire temperature range, which can be explained by the relation: $C_p - C_v = \alpha BVT$ (α = volume thermal expansion coefficient). At low temperatures, C_p exhibits Debye T^3 power-law behavior same as C_v , then C_p monotonously increases and deviates from C_v with increasing temperature. The difference between specific heats is due to the thermal expansion caused by anharmonicity effects.

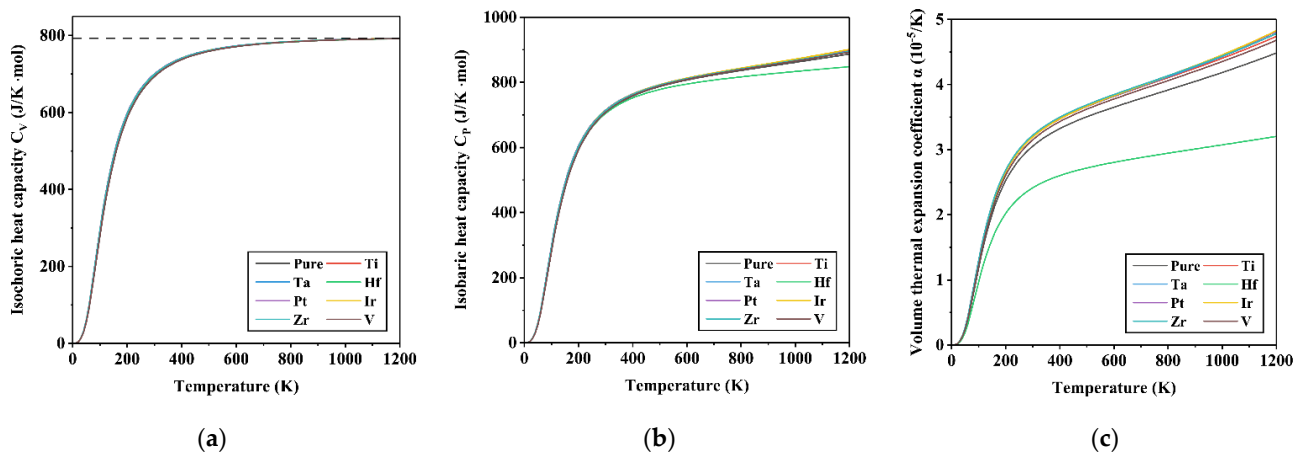


Figure 10. (a) Heat capacity at constant volume (C_v), (b) heat capacity at constant pressure (C_p) and (c) volume thermal expansion (α) of X-substituted Co_3Nb compounds ($X = \text{Ti}, \text{Ta}, \text{Hf}, \text{Pt}, \text{Ir}, \text{Zr}$ and V).

Finally, to estimate the effect of alloying elements on the volume change arise from temperature, the volume thermal expansion coefficient α of both the γ' - Co_3Nb and X-substituted γ' - Co_3Nb compounds at finite temperature was calculated, as shown in Figure 10c. For all X-substituted γ' - Co_3Nb compounds, the value of α increases sharply from 0K to about 300K, gradually approaching a linear increase at high temperatures, and the incremental trend becomes moderate. It is noteworthy that all γ' - Co_3Nb compounds show a similar trend with increasing temperature, except for the Hf-substituted γ' - Co_3Nb . The α of γ' - Co_3Nb substituted by Hf is much lower than that of γ' - Co_3Nb substituted by other elements, which means that addition of Hf element can effectively resist the volume effect of γ' - Co_3Nb caused by temperature.

4. Conclusions

In this study, we clarified the alloying effect on the atomic structure, elastic mechanical properties and relative phase stability of γ' - Co_3Nb compound by using DFT calculations. From the calculated transfer energy of various alloying elements in different sublattices of γ' - Co_3Nb , Y, Zr, Hf and Ta have a strong preference in Nb sites, while Ni, Rh, Pd, Ir and Pt are more inclined to occupy Co sites. For elements of the same period, the tendency to occupy Co site enhances with the increase of atomic number. In the ground state, the stabilizing effect of transition metal elements on γ' - Co_3Nb are listed in order as follows: $\text{Ti} > \text{Ta} > \text{Hf} > \text{Pt} > \text{Ir} > \text{Zr} > \text{Rh} > \text{V} > \text{Ni} > \text{W} > \text{Sc} > \text{Mo} > \text{Pd} > \text{Re} > \text{Ru}$. After comparing the shear modulus of different crystal planes, it is found that these X-substituted γ' - Co_3Nb are more likely to shear on the $\{110\}$ crystal plane along the $[1\bar{1}0]$ direction. The analysis of the electronic structure show that when the alloying element, such as Tc, occupies the Nb site, the ring-shaped electron distribution formed is beneficial to the improvement of the shear modulus. At finite temperatures, the addition of Ti, Ta, Hf, Pt, Ir, Zr and V can effectively expand the stabilization temperature range of γ' - Co_3Nb . In particular, the addition of Hf element can further reduce the sensitivity of the volume of γ' - Co_3Nb to temperature.

Supplementary Materials: The following are available online at <https://www.mdpi.com/article/10.3390/met11060933/s1>, Figure S1: Crystal structure of D019-ordered Co_3Nb , Table S1: Calculated structural properties for D019- Co_3Nb phase with transition element X doped.

Author Contributions: Conceptualization, C.W. and X.L.; data curation, C.Z. and Y.W.; formal analysis, C.Z. and W.X.; investigation, C.Z., Y.W. and J.H.; methodology, J.H.; resources, C.W. and X.L.; software, C.Z. and Y.W.; supervision, C.W. and X.L.; visualization, C.Z. and Y.W.; writing—original draft, C.Z., Y.W. and J.H.; writing—review and editing, C.Z. and J.H. All authors have read and agreed to the published version of the manuscript.

Funding: This work was supported by the National Natural Science Foundation of China (Grant No. 51831007), and the National Key Research and Development Program of China (Grant No. 2017YFB0702901).

Data Availability Statement: Not applicable.

Conflicts of Interest: The authors declare there is no conflicts of interest regarding the publication of this paper.

References

1. Sims, C.T.; Stoloff, N.S.; Hagel, W.C. *Superalloys II: High-Temperature Materials for Aerospace and Industrial Power*; J. Wiley & Sons: Hoboken, NJ, USA, 1987; pp. 2–5.
2. Reed, R.C. *The Superalloys: Fundamentals and Applications*; Cambridge University Press: Cambridge, UK, 2006; pp. 73–86.
3. Sato, J.; Omori, T.; Oikawa, K.; Ohnuma, I.; Kainuma, R.; Ishida, K. Cobalt-Base High-Temperature Alloys. *Science* **2006**, *312*, 90–91. [[CrossRef](#)]
4. Pollock, T.M.; Dibern, J.; Tsunekane, M.; Zhu, J.; Suzuki, A. New Co-based γ - γ' high-temperature alloys. *JOM* **2010**, *62*, 58–63. [[CrossRef](#)]
5. Suzuki, A.; DeNolf, G.C.; Pollock, T.M. Flow stress anomalies in γ/γ' two-phase Co–Al–W-base alloys. *Scr. Mater.* **2007**, *56*, 385–388. [[CrossRef](#)]
6. Suzuki, A. High-temperature strength and deformation of γ/γ' two-phase Co–Al–W-base alloys. *Acta Mater.* **2008**, *56*, 1288–1297. [[CrossRef](#)]
7. Lass, E.A.; Williams, M.E.; Campbell, C.E.; Moon, K.-W.; Kattner, U.R. γ' Phase Stability and Phase Equilibrium in Ternary Co–Al–W at 900 °C. *J. Phase Equilibria Diffus.* **2014**, *35*, 711–723. [[CrossRef](#)]
8. Bocchini, P.J.; Sudbrack, C.K.; Noebe, R.D.; Dunand, D.C.; Seidman, D.N. Effects of titanium substitutions for aluminum and tungsten in Co-10Ni-9Al-9W (at%) superalloys. *Mater. Sci. Eng. A* **2017**, *705*, 122–132. [[CrossRef](#)]
9. Makineni, S.; Samanta, A.; Rojhirunsakool, T.; Alam, T.; Nithin, B.; Singh, A.; Banerjee, R.; Chattopadhyay, K. A new class of high strength high temperature Cobalt based γ - γ' Co–Mo–Al alloys stabilized with Ta addition. *Acta Mater.* **2015**, *97*, 29–40. [[CrossRef](#)]
10. Makineni, S.; Nithin, B.; Chattopadhyay, K. Synthesis of a new tungsten-free γ - γ' cobalt-based superalloy by tuning alloying additions. *Acta Mater.* **2015**, *85*, 85–94. [[CrossRef](#)]
11. Im, H.J.; Makineni, S.K.; Gault, B.; Stein, F.; Raabe, D.; Choi, P.-P. Elemental partitioning and site-occupancy in γ/γ' forming Co–Ti–Mo and Co–Ti–Cr alloys. *Scr. Mater.* **2018**, *154*, 159–162. [[CrossRef](#)]
12. Zenk, C.H.; Povstugar, I.; Li, R.; Rinaldi, F.; Neumeier, S.; Raabe, D.; Göken, M. A novel type of Co–Ti–Cr-base γ/γ' superalloys with low mass density. *Acta Mater.* **2017**, *135*, 244–251. [[CrossRef](#)]
13. Ruan, J.; Liu, X.; Yang, S.; Xu, W.; Omori, T.; Yang, T.; Deng, B.; Jiang, H.; Wang, C.; Kainuma, R.; et al. Novel Co–Ti–V-base superalloys reinforced by L12-ordered γ' phase. *Intermetallics* **2018**, *92*, 126–132. [[CrossRef](#)]
14. Tirado, F.L.R.; Toinin, J.P.; Dunand, D.C. $\gamma+\gamma'$ microstructures in the Co–Ta–V and Co–Nb–V ternary systems. *Acta Mater.* **2018**, *151*, 137–148. [[CrossRef](#)]
15. Tirado, F.L.R.; Taylor, S.; Dunand, D.C. Effect of Al, Ti and Cr additions on the γ - γ' microstructure of W-free Co–Ta–V-Based superalloys. *Acta Mater.* **2019**, *172*, 44–54. [[CrossRef](#)]
16. Ruan, J.; Xu, W.; Yang, T.; Yu, J.; Yang, S.; Luan, J.; Omori, T.; Wang, C.; Kainuma, R.; Ishida, K.; et al. Accelerated design of novel W-free high-strength Co-base superalloys with extremely wide γ/γ' region by machine learning and CALPHAD methods. *Acta Mater.* **2020**, *186*, 425–433. [[CrossRef](#)]
17. Chen, Y.; Wang, C.; Ruan, J.; Omori, T.; Kainuma, R.; Ishida, K.; Liu, X. High-strength Co–Al–V-base superalloys strengthened by γ' -Co₃(Al,V) with high solvus temperature. *Acta Mater.* **2019**, *170*, 62–74. [[CrossRef](#)]
18. Kirklin, S.; Saal, J.E.; Hegde, V.I.; Wolverton, C. High-throughput computational search for strengthening precipitates in alloys. *Acta Mater.* **2016**, *102*, 125–135. [[CrossRef](#)]
19. Nyshadham, C.; Oses, C.; Hansen, J.E.; Takeuchi, I.; Curtarolo, S.; Hart, G.L. A computational high-throughput search for new ternary superalloys. *Acta Mater.* **2017**, *122*, 438–447. [[CrossRef](#)]
20. Omori, T.; Oikawa, K.; Sato, J.; Ohnuma, I.; Kattner, U.R.; Kainuma, R.; Ishida, K. Partition behavior of alloying elements and phase transformation temperatures in Co–Al–W-base quaternary systems. *Intermetallics* **2013**, *32*, 274–283. [[CrossRef](#)]
21. Bocchini, P.J.; Sudbrack, C.K.; Noebe, R.D.; Dunand, D.; Seidman, D.N. Microstructural and creep properties of boron- and zirconium-containing cobalt-based superalloys. *Mater. Sci. Eng. A* **2017**, *682*, 260–269. [[CrossRef](#)] [[PubMed](#)]
22. Zhang, Y.; Fu, H.; Zhou, X.; Zhang, Y.; Xie, J. Enhanced mechanical properties of wrought γ' -strengthened Co-base superalloys by adjusting the relative content of Al and Ti. *Intermetallics* **2019**, *112*, 106543. [[CrossRef](#)]
23. Yan, H.-Y.; Vorontsov, V.; Dye, D. Alloying effects in polycrystalline γ' strengthened Co–Al–W base alloys. *Intermetallics* **2014**, *48*, 44–53. [[CrossRef](#)]
24. Jiang, C.; Gleeson, B. Site preference of transition metal elements in Ni₃Al. *Scr. Mater.* **2006**, *55*, 433–436. [[CrossRef](#)]
25. Ruban, A.V.; Popov, V.; Portnoi, V.; Bogdanov, V. First-principles study of point defects in Ni₃Al. *Philos. Mag.* **2013**, *94*, 20–34. [[CrossRef](#)]

26. Stevanović, V.; Lany, S.; Zhang, X.; Zunger, A. Correcting density functional theory for accurate predictions of compound enthalpies of formation: Fitted elemental-phase reference energies. *Phys. Rev. B* **2012**, *85*, 115104. [[CrossRef](#)]
27. Shang, S.; Wang, Y.; Liu, Z.-K. First-principles elastic constants of α - and θ -Al₂O₃. *Appl. Phys. Lett.* **2007**, *90*, 101909. [[CrossRef](#)]
28. Chung, D.H. The Voigt-Reuss-Hill Approximation and Elastic Moduli of Polycrystalline MgO, CaF₂, β -ZnS, ZnSe, and CdTe. *J. Appl. Phys.* **1967**, *38*, 2535. [[CrossRef](#)]
29. Kresse, G.; Furthmüller, J. Efficient iterative schemes for ab initio total-energy calculations using a plane-wave basis set. *Phys. Rev. B* **1996**, *54*, 11169–11186. [[CrossRef](#)] [[PubMed](#)]
30. Kresse, G.; Furthmüller, J. Efficiency of ab-initio total energy calculations for metals and semiconductors using a plane-wave basis set. *Comput. Mater. Sci.* **1996**, *6*, 15–50. [[CrossRef](#)]
31. Kresse, G.; Joubert, D. From ultrasoft pseudopotentials to the projector augmented-wave method. *Phys. Rev. B* **1999**, *59*, 1758–1775. [[CrossRef](#)]
32. Hohenberg, P.; Kohn, W. Inhomogeneous Electron Gas. *Phys. Rev.* **1964**, *136*, B864–B871. [[CrossRef](#)]
33. Perdew, J.P.; Burke, K.; Ernzerhof, M. Generalized gradient approximation made simple. *Phys. Rev. Lett.* **1996**, *77*, 3865–3868. [[CrossRef](#)]
34. Pauling, L. Atomic Radii and Interatomic Distances in Metals. *J. Am. Chem. Soc.* **1947**, *69*, 542–553. [[CrossRef](#)]
35. Dirand, L.; Cormier, J.; Jacques, A.; Chateau-Cornu, J.-P.; Schenk, T.; Ferry, O.; Bastie, P. Measurement of the effective γ/γ' lattice mismatch during high temperature creep of Ni-based single crystal superalloy. *Mater. Charact.* **2013**, *77*, 32–46. [[CrossRef](#)]
36. Ooshima, M.; Tanaka, K.; Okamoto, N.; Kishida, K.; Inui, H. Effects of quaternary alloying elements on the γ' solvus temperature of Co–Al–W based alloys with fcc/L12 two-phase microstructures. *J. Alloys Compd.* **2010**, *508*, 71–78. [[CrossRef](#)]
37. Wang, L.; Oehring, M.; Liu, Y.; Lorenz, U.; Pyczak, F. Site occupancy of alloying elements in the L12 structure determined by channeling enhanced microanalysis in γ/γ' Co-9Al-9W-2X alloys. *Acta Mater.* **2019**, *162*, 176–188. [[CrossRef](#)]
38. Xu, W.; Shang, S.; Wang, C.; Gang, T.; Huang, Y.; Chen, L.; Liu, X.; Liu, Z. Accelerating exploitation of Co-Al-based superalloys from theoretical study. *Mater. Des.* **2018**, *142*, 139–148. [[CrossRef](#)]
39. Born, M. Thermodynamics of Crystals and Melting. *J. Chem. Phys.* **1939**, *7*, 591–603. [[CrossRef](#)]
40. De Jong, M.; Chen, W.; Notestine, R.; Persson, K.; Ceder, G.; Jain, A.; Asta, M.; Gamst, A. A Statistical Learning Framework for Materials Science: Application to Elastic Moduli of k-nary Inorganic Polycrystalline Compounds. *Sci. Rep.* **2016**, *6*, 34256. [[CrossRef](#)] [[PubMed](#)]
41. Pugh, S. XCII. Relations between the elastic moduli and the plastic properties of polycrystalline pure metals. *Lond. Edinb. Dublin Philos. Mag. J. Sci.* **1954**, *45*, 823–843. [[CrossRef](#)]
42. Pettifor, D.G. Theoretical predictions of structure and related properties of intermetallics. *Mater. Sci. Technol.* **1992**, *8*, 345–349. [[CrossRef](#)]
43. Knowles, K.M.; Howie, P.R. The Directional Dependence of Elastic Stiffness and Compliance Shear Coefficients and Shear Moduli in Cubic Materials. *J. Elast.* **2015**, *120*, 87–108. [[CrossRef](#)]
44. Wang, C.; Yan, L.; Han, J.; Xu, W.; Deng, B.; Liu, X. Effects of alloying elements on the structural, elastic and thermodynamic properties of Co₃Ta compounds from first-principles calculations. *J. Alloys Compd.* **2017**, *726*, 490–497. [[CrossRef](#)]
45. Xu, W.; Han, J.; Wang, Y.; Wang, C.; Liu, X.; Liu, Z.-K. First-principles investigation of electronic, mechanical and thermodynamic properties of L12 ordered Co₃(M, W) (M=Al, Ge, Ga) phases. *Acta Mater.* **2013**, *61*, 5437–5448. [[CrossRef](#)]
46. Blanco, M.; Francisco, E.; Luaña, V. GIBBS: Isothermal-isobaric thermodynamics of solids from energy curves using a quasi-harmonic Debye model. *Comput. Phys. Commun.* **2004**, *158*, 57–72. [[CrossRef](#)]
47. Otero-De-La-Roza, A.; Abbasi-Pérez, D.; Luaña, V. Gibbs2: A new version of the quasiharmonic model code. II. Models for solid-state thermodynamics, features and implementation. *Comput. Phys. Commun.* **2011**, *182*, 2232–2248. [[CrossRef](#)]